Unrevealing the Impact of Annealing Condition on Catalytic Activity of PtNi Alloy Electrode Towards Oxygen Reduction Reaction

Anindya Pramudya Wardhani[1], Salwaa Tanaya[2], Retna Deca Pravitasari[3], Damisih Damisih[3], Dewi Kusuma Arti[3], Sri Rahayu[4], Muhammad Didik Gumelar[4], and Elok Fidiani[1*]

[1]Department of Physics, Parahyangan Catholic University, Jl. Ciumbuleuit 94, Bandung 40141, Indonesia

[2]Department of Chemical Engineering, Parahyangan Catholic University, Jl. Ciumbuleuit 94, Bandung 40141, Indonesia

[3]Research Center for Advanced Materials, National Research and Innovation Agency (BRIN), Jl. Raya Puspiptek 60, Setu, Tangerang Selatan 15314, Indonesia

[4]Research Center for Energy Conversion and Conservation, National Research and Innovation Agency (BRIN), Jl. Raya Puspiptek 60, Setu, Tangerang Selatan 15314, Indonesia

Abstract: *Alloying platinum (Pt) with transition metals such as nickel (Ni) has been an effective approach for reducing Pt loading and enhancing catalytic activities towards the sluggish oxygen reduction reaction (ORR) on the cathode of proton exchange membrane fuel cell (PEMFC). In this work, we advance the fabrication of PtNi alloy electrodes through direct synthesis on the gas diffusion layer (GDL) utilizing wet chemical reduction methods. The catalytic activities and binding interaction between Pt and Ni are optimized through annealing PtNi electrodes at 200 °C under different gas flows of N_2 and the mixture of H_2/N_2 at 5%/95%. The physical characterization using X-ray diffraction (XRD) analysis and scanning electron microscope-energy dispersive X-ray spectroscopy (SEM-EDX) show the significant effect of the annealing environment on the morphology and distribution of the PtNi alloy catalyst on the GDL surface. The optimized electrodes exhibited enhanced ORR mass activity, with values of 8.17 and 18.26 mA mg^{-1} for PtNi annealed with N_2 and N_2/H_2, respectively, surpassing the benchmark Pt/C (5.25 mA mg^{-1}). These results underscore the critical role of the annealing environment in optimizing the catalytic performance of PtNi-based electrodes for PEMFC applications, offering insights into more efficient fuel cell technologies.*

Keywords: *PtNi; ORR; PEMFC; annealing; catalyst electrode*

■ INTRODUCTION

Fuel cells are considered promising and environmentally friendly technologies for replacing fossil fuel-based generators due to their clean conversion mechanism from hydrogen (H_2) [1]. Among some types of fuel cells, proton exchange membrane fuel cells (PEMFCs) have been commercialized for fuel cell hydrogen electric vehicles (FCHEVs) due to their high efficiency and power density at low operating temperatures [2-3]. However, due to its high activation energy, a significant challenge in PEMFCs is addressed to the slow oxygen reduction reaction (ORR) mechanism at the cathode side [4]. This reaction involves multiple electron transfer steps, the breaking and forming of O–O bonds, and the adsorption of O_2 on the electrode surface. As a result, cathode PEMFCs require high-loading platinum (Pt) catalysts, leading to the high-cost production of PEMFC technology [5-6]. Over the past decades, extensive research and development efforts have focused on improving the catalytic activities of electrodes for the ORR and minimizing the use of Pt by alloying with more abundant and cheap metals such as nickel (Ni) [7-8], cobalt (Co) [9-10], silver (Ag), etc. [11-12].

Developing a Pt-based alloy catalyst electrode has proven to be an effective approach for reducing the amount of Pt and enhancing the ORR activity [13]. The significance of Pt alloying with other metals is primarily attributed to modifications in surface properties, resulting from changes in the distance between Pt–Pt atoms and bonding dynamic between Pt and the hybrid metals, which further improve the catalytic activities towards ORR [14-15]. The theoretical calculation and experimental report showed that alloying Pt with Ni generates the highest ORR activity at the cathode of PEMFCs [16]. Markovic et al. [17] reported that Pt_3Ni (111) exhibits a ten-fold higher ORR activity compared to monometallic Pt (111) and a 90-fold higher activity compared to commercial Pt/C. An advanced de-alloying method has been developed to construct a Pt_3Ni nanoframe catalyst with a Pt-skin, achieving an impressive mass activity of 5.7 A mg_{Pt}^{-1} [7]. This open-structured design maximizes the catalyst's surface-to-volume ratio, enhancing accessibility for electrochemical reactions. Furthermore, the highly active, shape-controlled Pt_3Ni (111) catalyst, along with Mo-doped Pt_3Ni octahedral, demonstrates exceptional ORR activities up to 73 times higher than those of commercial Pt/C catalysts [18].

However, these impressive catalyst activity results were primarily achieved through ex-situ half-cell tests using the rotating disk electrode (RDE) technique in liquid electrolytes. To date, only a limited number of PtNi catalysts have been successfully transferred to membrane electrode assemblies (MEAs) for practical PEMFC applications. This limitation arises from the significant challenges in reproducing their high catalytic activity under real fuel cell operating conditions, as well as the difficulties associated with scaling up production for mass deployment [19]. Therefore, designing the rationale and stable structure of PtNi-based catalyst electrodes, along with the facile synthesis method for scalable production, is important, and this is the focus of this research. Furthermore, a comprehensive study on developing Ni-based catalysts can potentially expand the successful PEMFC application in Indonesia, considering that Indonesia is one of countries with the largest Ni reserves in the world [20].

In this work, we synthesize the PtNi alloy catalyst directly on the gas diffusion layer (GDL) substrate, adapting the previous work by Mardle et al. [21]. This facile scalable method utilizes the formic acid reduction approach to promote the formation of support-free PtNi nanostructures on the GDL. However, the PtNi alloy structure frequently causes a higher degree of segregation due to the lattice mismatch between Pt and Ni, causing performance loss during PEMFC operation [9,18]. Post-treatment to optimize the Pt-Ni property is commonly achieved through annealing in reductive conditions [22-23]. Annealing promotes the formation of highly active PtNi nanostructures by preventing oxidation and facilitating the reduction of surface oxides, thereby improving the catalyst's ORR performance. Hence, carefully controlling the annealing atmosphere is essential in the synthesis of high-performance electrocatalysts for PEMFCs.

In this study, we aim to elucidate the role of annealing environments on the performance of PtNi alloy electrodes for PEMFC applications. We specifically investigate the effects of varying the gas flow composition between pure N_2 and a mixture of H_2 and N_2 during annealing. By investigating the altering of these conditions, we seek to understand how different annealing atmospheres influence the physical and catalytic properties of PtNi alloy electrodes. Furthermore, the ORR performance is evaluated using a gas diffusion electrode (GDE) half-cell setup, enabling full electrode measurements under conditions more representative of MEA testing. Our goal is to provide a comprehensive analysis of the environmental variations that affect the structural and catalytic characteristics of PtNi alloy electrodes, ultimately aiming to enhance their performance toward ORR for application in PEMFC.

■ EXPERIMENTAL SECTION

Materials

Chloroplatinic acid (H_2PtCl_6 8 wt.% H_2O), nickel chloride hexahydrate ($NiCl_2 \cdot 6H_2O$), formic acid (HCO_2H 99%), sodium borohydrade ($NaBH_4$ 98%), nitric acid (HNO_3 70%), 2-butanol (IPA), and nafion solution 10 wt.% in H_2O were all purchased from Sigma-

Aldrich, Germany. Carbon paper Sigracet 39 BB (FuelCell Store, USA) was used as GDLs. The water used in this work is purified and purchased from OneMed, Indonesia. Perchloric acid ($HClO_4$, 70–72%) was purchased from Merck, Germany, as the electrolyte for the half-cell electrochemical measurements.

Instrumentation

To obtain the metal loading of PtNi on GDL, thermogravimetric analysis (TGA, LABSYS evo, France) was conducted with a heating rate of 10 °C/min from room temperature until 900 °C under O_2 gas flow. For TGA analysis, the electrode of PtNi/GDL was cut to 1×1 cm^2 and then placed in the crucible. The amount of PtNi was obtained from the final mass of the measured residue. X-ray diffraction (XRD, Rigaku SmartLab, Japan) analysis was carried out to analyze the structure and alloying degree of PtNi/GDL electrode with Cu X-ray sources ($\lambda = 0.15406$ nm) between 10–90°. Scanning electron microscope conjugated with energy-dispersive X-ray (SEM-EDX, Jeol JSM-IT200, Japan) analysis was used to analyze the morphology of PtNi/GDL electrode and obtain the atomic ratio of Pt and Ni. Field emission SEM (FE-SEM, Jeol JIB-4610F, Japan) was also used to generate high-magnification images of the PtNi catalyst structure on the GDL.

Procedure

Synthesis of PtNi alloy on GDL

The synthesis procedure of PtNi utilizes the wet chemical reduction method adapting the previous work by Mardle et al. [21]. The GDL Sigracet 39 BB, with the size of 5×5 cm^2 was first activated by soaking it in the petri dish filled with H_2O, followed by rinsing it with H_2O and IPA. A 16.5 mL of H_2O was then added and let the GDL sink at the bottom of the petri dish. The H_2PtCl_6 solution was added dropwise into the petri dish, and then the mixture was sonicated on a sonication bath for around 1 min, followed by adding 830 μL of HCO_2H dropwise during sonication time of ca. 1 min at room temperature. The lid was then placed to cover the petri dish and stored at 40 °C for 72 h. The washing procedure was then carried out with IPA and H_2O, followed by the drying step in the oven at 40 °C for ca. 2 h.

To form PtNi alloy, Ni was synthesized directly on Pt/GDL with the atomic ratio of Pt:Ni = 4:3. Pt/GDL was painted with a solution of 100 μL H_2O mixed with 10.4 mg $NiCl_2 \cdot 6H_2O$ followed by painting a second solution made of 10.4 mg $NaBH_4$ mixed with 1 mL NaOH 0.1 M. The petri dish was covered by the lid and left at room temperature for 2–3 h for the formation of Ni nanoparticles. The washing step of PtNi/GDL was then carried out with H_2O and IPA, followed by drying the sample at room temperature. PtNi/GDL was then treated with thermal annealing in a tube furnace at 200 °C for 24 h under the varied gas flow of N_2 and the mixture of H_2/N_2 (5%/95%) with a gas flow of 50 mL min^{-1} flow. Acid treatment was then performed to clean up the surface of GDL from the impurities by submerging the PtNi/GDL in the 0.1 M HNO_3 for 2–3 h at RT. The PtNi/GDL electrode was then dried and ready for physical characterization and electrochemical testing.

GDE half-cell measurement

To examine the catalytic activity and performance of PtNi/GDL electrode (PtNi GDE) toward ORR, GDE-half cell electrochemical measurement was performed using FlexCell PP 83200 (Gaskatel Ltd., Germany) operated with Parstat 4000A (AmetekSI Ltd., USA). PtNi/GDL was first cut to 3×5 cm^2 followed by coating it with ionomer solution with a concentration of 0.6 mg cm^{-2}. The coated PtNi/GDL was then placed in the FlexCell as a working electrode (WE), and 0.1 M $HClO_4$ was added as an electrolyte solution into the chamber. The cable was then connected to the counter and reference electrode, followed by flowing N_2 into a gas chamber on the WE side at a rate of 100 mL min^{-1} for around 45 min or until the chamber was fully saturated. The cyclic voltammetry (CV) was first run as an activation or cleaning step with a scan rate of 200 mV s^{-1} for up to 50 cycles between 0.05–1.20 V vs. reversible hydrogen electrode (RHE). The 3 cycles of CVs were then generated with a scan rate of 100 mV s^{-1} between 0.05–1.20 V vs. RHE, which is used as the primary data to measure the electrochemical surface area (ECSA).

The Pt nanowire (PtNW) GDE performance toward ORR was then measured using a polarization

curve, which was obtained following the method explained by Ehelebe et al. [24-25]. The gas flow into the chamber was first switched to O_2 with the same flow rate of 100 mL min^{-1} until the saturated condition was reached or ca. 30 min. The polarization curve was then generated by applying the Galvanostatic steps coupled with impedance spectroscopy (GEIS) and was run from −0.15 mA until reaching the optimum value (during this work, the optimum value was reached at −750 mA). The obtained voltage of every step was corrected with the internal ohmic resistance (iR) generated from impedance spectroscopy run between the frequency range of 100 kHz–10 Hz and an amplitude of 5 mA cm^{-2}. The determination of the iR value is based on the intercept of the curve with the real x-axis at the high-frequency region. The kinetic current from the corrected polarization curve was measured at 0.9 V vs. RHE to determine the ORR mass activity.

■ RESULTS AND DISCUSSION

Physical Characterization

SEM images in Fig. 1 show the surface morphology of the PtNi electrode. At low magnification (Fig. 1(a) and 1(d)), PtNi/GDL annealed with different gases of N_2 and H_2/N_2 show a similar structure and distribution of catalyst particles on the surface of the electrode. At higher magnification, SEM images in Fig. 1(b) and 1(c) reveal the higher degree of agglomerated catalyst particles for PtNi/GDL annealed with N_2 gas. Hence, the electrode surface exhibits an irregular structure and uneven distribution of the PtNi catalyst particles on the GDL surface. Meanwhile, the PtNi electrode treated with H_2/N_2 shows a more homogeneous distribution of particles on the surface of GDL, as shown in Fig. 1(e) and 1(f). This primarily occurs because H_2 is a reductive gas acting as a reducing agent. It effectively removes surface oxides that may form on the catalyst particles. In an inert N_2 atmosphere, the absence of a reducing agent allows surface oxides to persist, increasing the surface energy and promoting particle agglomeration as the system seeks to minimize this energy. Meanwhile, the H_2 in H_2/N_2 reduces these oxides, maintaining a clean metal surface with lower surface energy, which helps to prevent aggregation [26]. This result indicates a significant influence of the annealing environment on the structure and distribution of PtNi catalyst particles on the electrode.

Further observation on PtNi/GDL electrode treated with H_2/N_2 gas exhibits the distribution of particles with an average size of 100–250 nm (Fig. 2). The high-resolution SEM image in Fig. 2 reveals that the particles are composed of an assembly of one-dimensional (1D) nanostructures like NW array. Such a structure is commonly observed for Pt synthesized directly on GDL using a wet chemical reduction method using formic acid [27-29]. Furthermore, 1D nanomaterials such as NW and
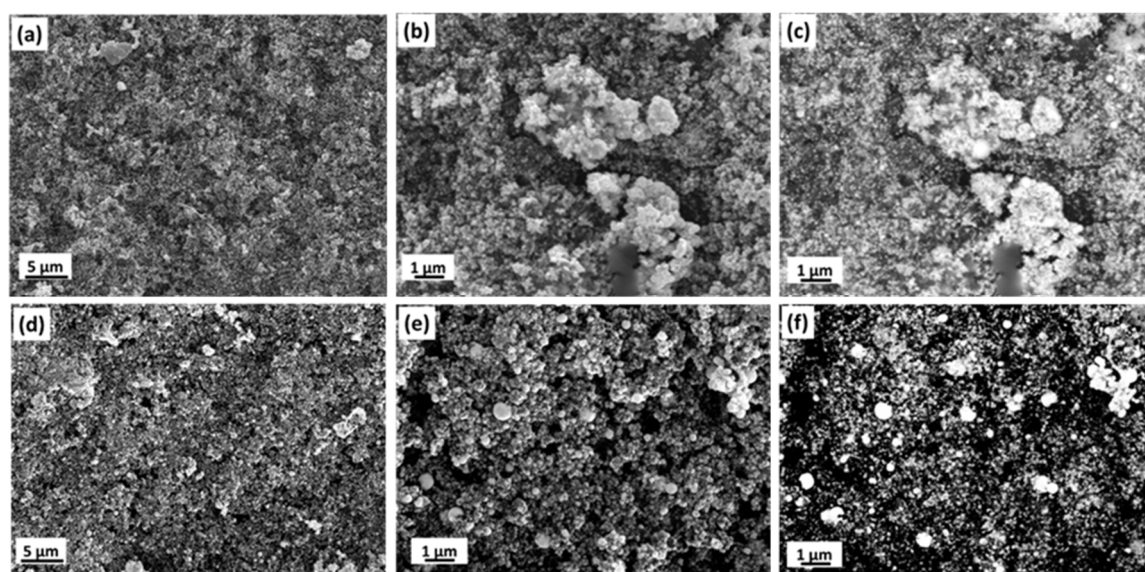

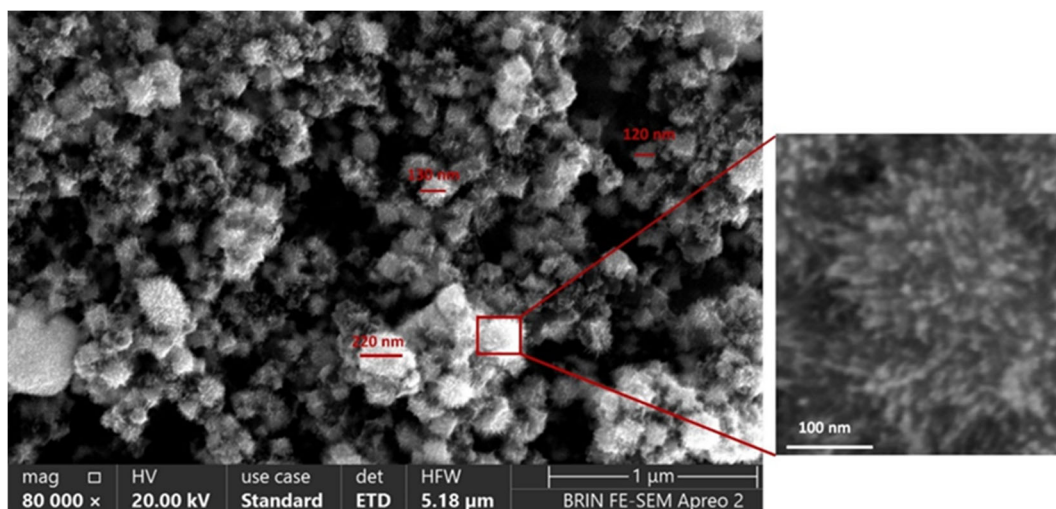**Fig 1.** SEM images of PtNi/GDL annealed with (a-c) N_2 and (d-f) H_2/N_2 gas

Fig 2. High-resolution SEM images of PtNi/GDL annealed with H_2/N_2 gas

nanorod (NR) highlight several advantages over nanoparticles (NPs), such as high active crystal facets (111) and high stability leading to higher catalytic activities towards the ORR than zero-dimensional (0D) Pt NPs [11]. The results of this study indicate that the incorporation of Ni and the annealing treatment in an H_2/N_2 environment effectively preserve the integrity of the NW array structure. This observation is consistent with previous studies on the annealing effects on the structure of Pt-alloys, where annealing at a maximum temperature of 200 °C was found to maintain the 1D structure of the Pt-based alloy catalysts [21-22].

The quantitative measurement on PtNi/GDL was carried out with TGA analysis run until 900 °C under O_2 gas flow to obtain the metal loading of PtNi deposited on the electrode. GDL is commonly composed of porous matrix substrates made of carbon-based materials, which should be entirely oxidized during TGA analysis under O_2 flow at a high temperature above 400 °C [30-31]. Hence, only the residue of the PtNi catalyst was left deposited on the GDL, as presented in Table 1. The theoretical loading of Pt based on the experimental procedure is about 0.38–0.42 mg cm^{-2}, and the additional mass above this value is expected to be the Ni component. The mass exhibited from TGA analysis for PtNi/GDL annealed with N_2 gas is 0.48 mg cm^{-2}, which is higher than the loading of 0.43 mg cm^{-2} observed for PtNi/GDL annealed with H_2/N_2 gas. This outcome suggests a higher Ni composition on the electrode for the sample treated with N_2 gas, as confirmed by EDX analysis and presented in Table 1.

The SEM-EDX mapping on the cross-section area of PtNi/ GDL is presented in Fig. 3, showing the domination of the Pt composition on the top area of the electrodes. The higher contrast for metal compounds is more distinguished for the electrode of PtNi/GDL treated with N_2 gas (Fig. 3(b) and 3(c)) than with H_2/N_2 one (Fig. 3(f) and 3(g)), further confirming the higher mass loading obtained from TGA analysis. The quantitative analysis using the EDX spectrum (Fig. 3(d) and 3(h)) shows the Ni compositions of ca. 1.5–2.0 atomic% for both electrodes, which are much smaller than than the theoretical mass designed in the experimental procedure of above 20 atomic%. It is potentially caused by

Table 1. The quantitative measurement of metal composition based on TGA and SEM-EDX

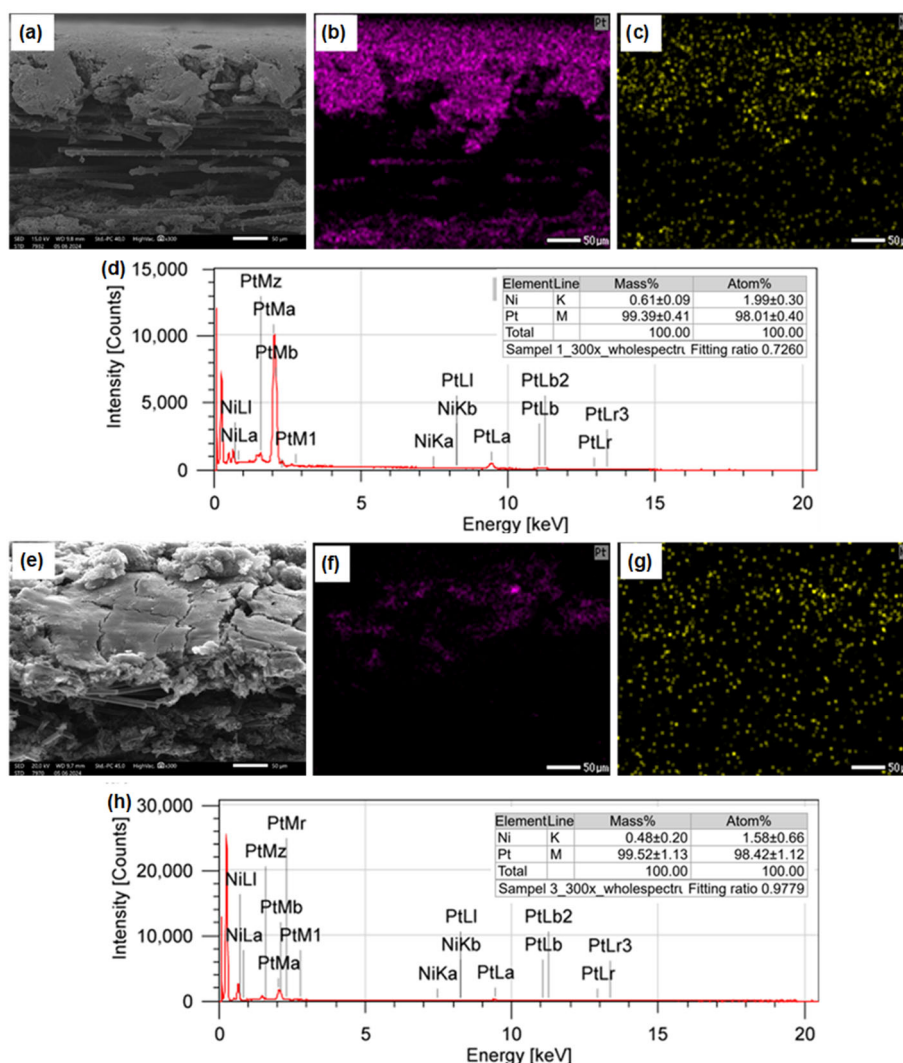| Sample	TGA (mg cm^{-2})	SEM-EDX	
		Pt (atomic%)	Ni (atomic%)
PtNi/GDL N_2	0.48	98.01	1.99
PtNi/GDL H_2/N_2	0.43	98.42	1.58
Pt/GDL	0.40	100	0

Fig 3. SEM-EDX mapping images on the cross-sectional area and corresponding EDX spectrum of PtNi/GDL annealed with (a-d) N_2 and (e-h) H_2/N_2 gas

the acid-leaching process performed after the annealing step.

Those outcomes suggest some possibilities. First, the annealing step at low temperatures of 200 °C is still less effective in strengthening the binding interaction between Pt and Ni, leading to the dissolution of the Ni compound during acid treatment. Hence, leaving only a small amount of Ni attached to Pt to form PtNi alloy. The acid treatment is intended to remove the impurities and excess amount of Ni to optimize the surface area on the surface of the catalyst layer [32]. However, transition metals like Ni exhibit poor stability, leading to spontaneous oxidation at low pH and susceptibility to leaching under acidic

conditions, which is further dissolved during this process [33]. Then, thermal annealing, especially in a reductive environment of H_2/N_2 gas, induces the atomic segregation of Pt to the surface, leading to the formation of a Pt-rich shell [21,34]. Therefore, only a small amount of Ni is detected, considering EDX is a surface analysis method, especially at low magnification. This presumption is validated by the high-magnification EDX analysis on the surface area of PtNi/GDL electrode annealed with H_2/N_2 gas shown in Fig. 4. A higher atomic ratio of Ni, up to 2.4 atomic%, is detected. This indicates that the higher energy beam is capable of penetrating deeper into the material's surface, thereby revealing a greater concentration of Ni
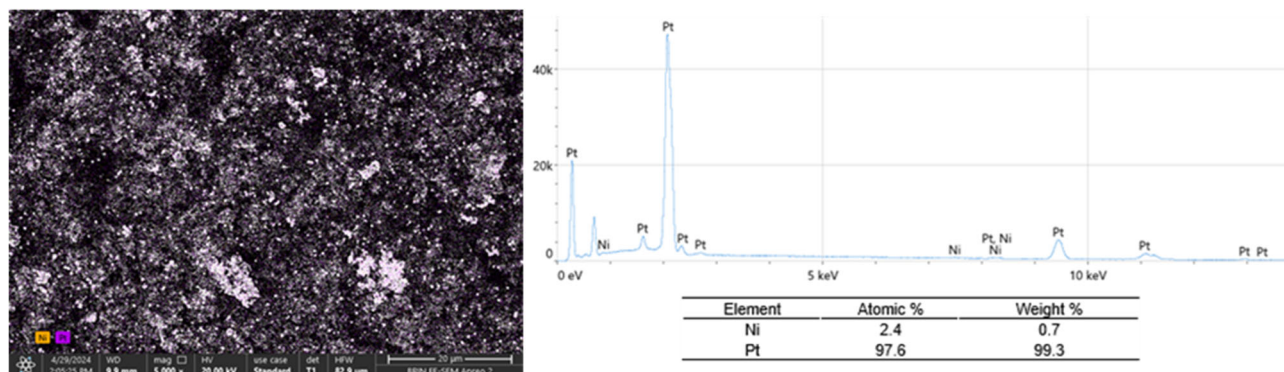
Fig 4. SEM-EDX mapping and spectrum on the surface of PtNi/GDL annealed with H_2/N_2 gas

deposits beneath the Pt shell. A similar analysis using high-resolution TEM has shown the presence of Ni inside Pt NW synthesized with a similar method [21]. This deeper analysis suggests a more substantial presence of Ni within the internal structure of the catalyst, which could have significant implications for the material's overall catalytic performance.

The XRD analysis was also performed to evaluate the structure of PtNi electrodes. The distinguished peaks at $2\theta = 26.6°$ (Fig. 5(a)) correspond to graphitic carbon, which is commonly observed on the GDL substrate [22,30]. The other prominent peaks assigned to (111), (200), and (220) planes are in alignment with the reference of Pt (JCPDS-04-0802), confirming the domination of Pt composition on the GDL. The intensity of the Pt (111) facet is the highest, commonly observed on the 1D Pt nanostructure in our previous works [29]. This

result indicates the formation of a 1D nanostructure structure, which is in agreement with the SEM image in Fig. 2.

The magnification area on the Pt (111) peak (Fig. 5(b)) shows that the main peaks of both PtNi electrodes are also aligned to Pt/GDL and the reference of Pt (JCPDS-04-0802) without shifting closer to the Ni reference peak of JCPDS: 04-0850. This can be attributed to a low Ni amount detected on the electrode of ca. 2 atomic% based on the EDX results in Fig. 3 and 4. Nevertheless, both peaks of PtNi electrodes are narrower than Pt/GDL and commercial Pt/C catalysts, indicating the formation of bigger particles due to alloying with Ni and annealing, which was commonly observed in previous studies [22,34].

The formation of PtNi alloy catalyst potentially affects the formation of bigger particles. However, the
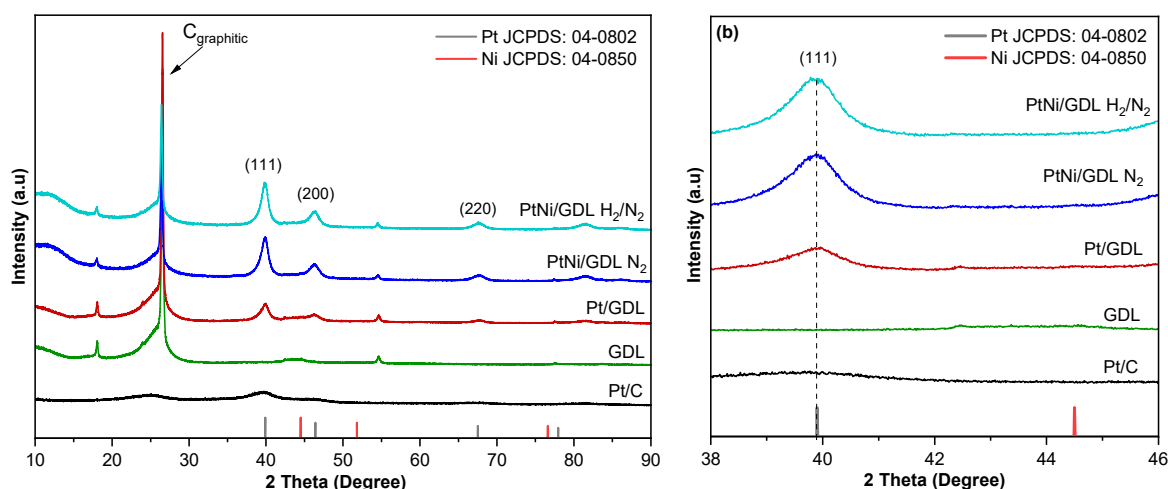

Fig 5. (a) XRD pattern and (b) high-resolution Pt (111) peaks of the as-made GDEs referencing Pt (JCPDS: 04-0802) and Ni (JCPDS: 04-0850)

effect of the annealing step toward the formation of bigger particle size is more prominent [35]. The XRD pattern peaks show that both electrodes of PtNi/GDL annealed with N_2 and H_2/N_2 gas exhibit a similar particle size. This suggests that environmental conditions have a less significant impact on the formation of larger particles. Instead, annealing temperature and time appear to play a more critical role in influencing particle size. This is due to the low resistance of Pt nanostructure toward heat treatment, suggesting optimizing the annealing temperature of 200 °C to minimize the aggregation [22]. Higher temperatures facilitate the growth of larger particles by providing the necessary energy for increased atomic mobility and agglomeration, especially with a long annealing period of up to 24 h. Nevertheless, the annealing step is crucial in optimizing the Pt and Ni interaction and minimizing the higher degree of atomic dissolution rendered by the lattice incongruity between Pt and Ni, which highly influences the catalytic activities towards ORR [9,36].

GDE Half-Cell Measurement

The *ex-situ* GDE half-cell measurement was conducted to examine the catalytic activity of GDE made of PtNi treated with N_2 and H_2/N_2 benchmarking to commercial Pt/C catalyst (20 wt.% Pt) and monometallic Pt grown directly on GDL (Pt/GDL). In this work, the Pt/C GDE was prepared by making the ink of the Pt/C catalyst and painted on the GDL with a loading of 0.4 mg_{Pt} cm^{-2}. Fig. 6 presents the CV of all tested GDEs obtained under N_2-saturated 0.1 M $HClO_4$ electrolyte with a scan rate of 100 mV s^{-1}. The current density observed on the CV of PtNi/GDL annealed in H_2/N_2 gas is the largest (Fig. 6(d)) compared to the other GDEs of Pt/GDL (Fig. 6(b)), PtNi/GDL N_2 (Fig. 6(c)) and even the commercial Pt/C (Fig. 6(a)), which relates to the increased number of active sites on the catalyst surface.

The ECSA was then measured from the hydrogen desorption region peak (H_{des}) between 0.05–0.40 V vs. RHE, as shown in the shaded region in Fig. 7. ECSA
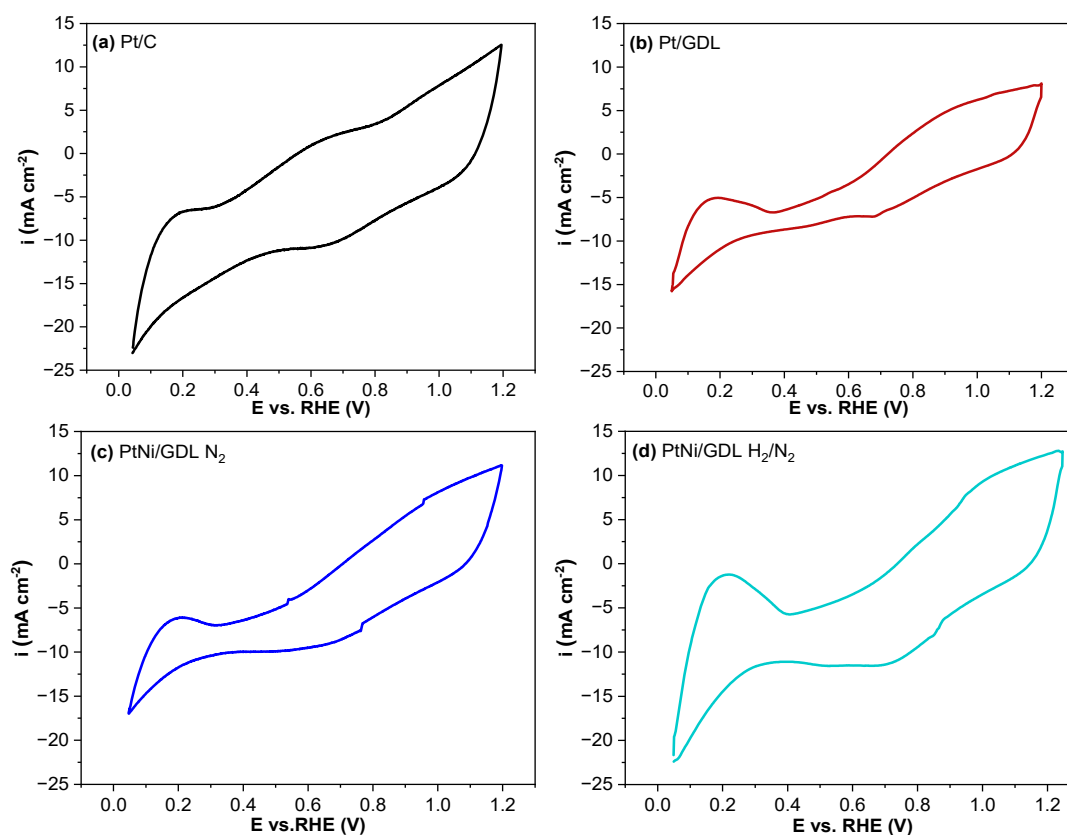

Fig 6. CV of (a) Pt/C, (b) Pt/GDL, PtNi/GDL annealed with (c) N_2 and (d) H_2/N_2 gas obtained in 0.1 M $HClO_4$ under N_2 gas flow with a scan rate of 100 mV s^{-1}
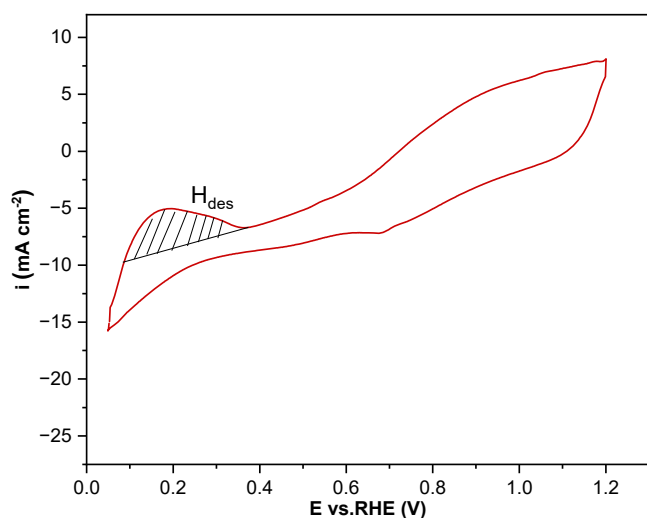
Fig 7. CV of Pt/GDL obtained in 0.1 M HClO₄ under N₂ gas flow with a scan rate of 100 mV s⁻¹

Table 2. The catalytic activities

Sample	ECSA (m² g⁻¹)	Mass Activity at 0.85 V vs. RHE (mA mg⁻¹)
Pt/C	42.67	5.25
Pt/GDL	28.76	14.18
PtNi/GDL N₂	18.28	8.17
PtNi/GDL H₂/N₂	30.06	18.26

represents the number of active sites accessible on the catalyst's surface, which can be determined from the Eq. (1);

$$ECSA = \frac{Q_{Hdes}}{m \times 210\ \mu C\ cm^{-2}} \qquad (1)$$

Q_{Hdes} is the charge linked to the chemical process measured from the H_{des} region shown in Fig. 7, converted to a current plot against time [37], m is the catalyst loading (PtNi) measured in grams, and the value of 210 μC cm⁻² is a conversion factor for the charge required to facilitate the reduction of hydrogen atoms on a polycrystalline Pt surface. The obtained ECSA is presented in Table 2 generated from the CVs in Fig. 6.

The measured ECSA of monometallic Pt/C and Pt/GDL are 42.67 and 28.76 m² g⁻¹, respectively. The ECSA value obtained for the benchmark Pt/C is in close agreement with the references [24,38], signifying the reliable technique applied in this work. These outcomes indicate that Pt synthesized directly on GDL provides a higher number of active sites on the catalyst layer. Adding

Ni to Pt/GDL to form PtNi/GDL alloy, along with the type of annealing gas used, significantly influences the ECSA. Specifically, PtNi/GDL annealed with a mixture of H₂/N₂ gas generates an ECSA of 30.06 m² g⁻¹, which is higher than that of PtNi/GDL treated with N₂ gas (18.28 m² g⁻¹). This result further affirms the positive effect of alloying Ni with Pt in providing more active sites available for ORR. This outcome refers to the positive effect of the annealing step under a reductive atmosphere of saturated H₂/N₂ to optimize the surface area. The presence of surfactant is potentially reduced during annealing, enhancing the catalyst properties. Furthermore, the annealing in a reductive atmosphere such as H₂ induces surface segregation due to differences in free energy, typically causing Pt to migrate to the surface, resulting in improved ECSA [34,36,39].

The polarization curves illustrating the ORR performances of the tested GDEs are presented in Fig. 8(a). The curves were generated in O₂-saturated 0.1 M HClO₄ with the GEIS method following the benchmarking procedure described by Ehelebe et al. [24-25]. The ORR activity metric refers to either the intrinsic activity normalized to the catalyst's electrochemical surface area (μA cm⁻²), known as specific activity, or the activity quantified per unit of mass (mA mg⁻¹) referred to as mass activity. For practical applications, mass activity is more prominent because it relates to the amount of Pt used, which is directly proportional to the manufacturing cost. Therefore, mass activity is one of the main parameters utilized in this work to determine the ORR activity. Mass activity is commonly measured from the kinetic current obtained between 0.9–0.85 V vs. RHE generated from the Tafel plots (the inset in Fig. 8(a)) [21,28,40]. In this work, the ORR current value is measured at 0.85 V vs. RHE.

A modest increase in mass activities is observed for all GDEs made by direct catalyst synthesis on GDL compared to Pt/C (Table 2). The GDE made of PtNi/GDL treated with H₂/N₂ generates mass activity of 18.26 mA mg⁻¹, which is higher than of PtNi/GDL treated with the N₂ gas (8.17 mA mg⁻¹) and Pt/GDL (14.18 mA mg⁻¹). The improvement in ORR kinetic activities is significant after adding Ni to Pt/GDL, followed
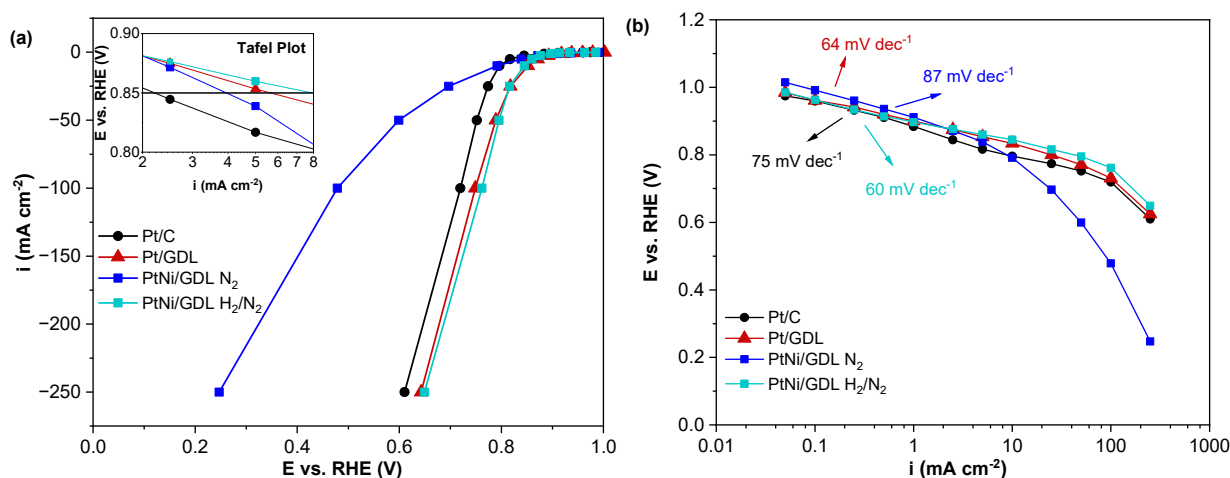
Fig 8. (a) Polarization curves and (b) corresponding Tafel plots of the GDEs made of Pt/C, Pt/GDL, PtNi GDL annealed with N_2, and mixed gas of H_2/N_2 generated in O_2-saturated 0.1 M $HClO_4$

by annealing with H_2/N_2. The PtNi/GDL treated with H_2/N_2 also exhibited the lowest Tafel slope of 60 mV dec^{-1} (Fig 8(b)), highlighting its faster kinetic performance in the ORR [41]. This enhanced performance is attributed to the cleaner catalyst surface and improved catalyst dispersion facilitated by reductive annealing conditions using H_2/N_2 gas. This optimizes the active site accessibility and accelerates the ORR reaction kinetics. In contrast, the PtNi/GDL annealed in N_2 showed a significantly higher Tafel slope of 87 mV dec^{-1} (Fig 8(b)), indicating slower reaction kinetics. The higher Tafel slope may result from a less effective catalyst distribution and potential surface contamination, which hinders the ORR process. These findings underscore the critical role of the annealing atmosphere in shaping the electrode's catalytic properties, confirming that a reductive environment like H_2/N_2 is essential for achieving faster and more efficient ORR kinetics.

At the operational fuel cell voltage of 0.6–0.7 V vs. RHE, the ORR performance trend follows PtNi/GDL H_2/N_2 > Pt/GDL > Pt/C > PtNi/GDL N_2, as shown in Fig. 8(a). A higher overpotential at a high reaction rate indicates mass transport limitation inducing the performance decrease. The significant performance drop of PtNi/GDL annealed with N_2 gas at high current density suggests this issue, indicating higher resistance slowing down the gas and reactant movement throughout the electrode. This is potentially rendered by higher agglomerated catalyst particles on the GDL surface, as observed in Fig. 1(b) and 1(c), blocking the transport of gas and reactant across the electrode.

Those results suggest that annealing PtNi/GDL with H_2/N_2 gas generates the highest overall performance toward ORR. This significant outcome can be attributed to the larger ECSA due to alloying with Ni and annealing in the reductive environment of H_2/N_2. The integration of Ni to form PtNi alloy induces surface modification on Pt, which is caused by the change of Pt–Pt bond distance and the bonding interaction between Pt and the alloyed metals, which results in improved kinetic activities towards ORR [42]. Furthermore, a good distribution and uniform size of catalyst particles, as presented in SEM images in Fig. 2(e) and 2(f), provide a smooth gas and mass transport throughout the electrode, minimizing mass transport issues at the high current density region. Finally, the optimized annealing condition in a reductive environment of H_2/N_2 demonstrates a significant impact on the integration of Ni to form PtNi alloy, thereby enhancing the catalytic performance toward ORR. It also greatly influences particle distribution and size, conferring a critical advantage, particularly in mitigating mass transport limitations. These findings have shown an effective strategy for the advanced fabrication of electrodes for PEMFC application.

CONCLUSION

In conclusion, this study demonstrates that the annealing environment significantly impacts the physical characteristics of PtNi electrodes, which greatly influence their catalytic activities, especially towards ORR. The reductive annealing environment of H_2/N_2 induces catalyst surface modification, resulting in a larger ECSA and enhancing the kinetics activities toward ORR. SEM-EDX characterization reveals that a reductive annealing environment involving H_2 facilitates a more uniform distribution of catalyst particles, reducing agglomeration and enhancing surface coverage. The XRD analysis confirms the alloy structure of PtNi and highlights the influence of annealing on crystallite size and phase composition. The well-distributed and uniformly sized catalyst particles are generated for the PtNi electrode annealed with H_2/N_2 gas. This is the key to facilitating smooth mass transport throughout the electrode, thus minimizing the overpotential at the fuel cell operational voltage. These findings further signify the importance of an annealing environment to optimize the catalytic performance of Pt-based alloy nanostructure electrodes for PEMFC application. Future studies could further explore the synergistic effects of different alloying elements and annealing atmospheres to push the boundaries of catalytic activities toward ORR.

ACKNOWLEDGMENTS

CONFLICT OF INTEREST

The authors declare no competing financial interest.

AUTHOR CONTRIBUTIONS

Anindya Pramudya Wardhani and Salwaa Tanaya undertook the experimental work, electrochemical testing, and manuscript preparation. Retna Deca Pravita Sari assisted in conducting physical characterizations and contributed to the manuscript revision. Damisih and Dewi Kusuma Arti assisted in conducting experiments. Sri Rahayu and Muhammad Didik Gumilar contributed to the data analysis and manuscript revisions. Elok Fidiani provided supervision, conceptualization, methodology, data analysis, and writing editing. All authors have approved the final version of the manuscript.

REFERENCES

[1] Fan, L., Tu, Z., and Chan, S.H., 2023, Recent development in design a state-of-art proton exchange membrane fuel cell from stack to system: Theory, integration and prospective, *Int. J. Hydrogen Energy*, 48 (21), 7828–7865.

[2] Alaswad, A., Baroutaji, A., Achour, H., Carton, J., Al Makky, A., and Olabi, A.G., 2016, Developments in fuel cell technologies in the transport sector, *Int. J. Hydrogen Energy*, 41 (37), 16499–16508.

[3] Das, P.K., Barbir, F., Jiao, K., Wang, Y., and Li, X., 2023, Fuel Cells for Transportation—An Overview in *Fuel Cells for Transportation*, Woodhead Publishing, Cambridge, MA, US, 1–28.

[4] Bard, A.J., and Faulkner, L.R., 2001, *Electrochemical Methods: Fundamentals and Applications*, 2nd Ed., Harris, John Wiley & Sons, New York, US.

[5] Pollet, B.G., Kocha, S.S., and Staffell, I., 2019, Current status of automotive fuel cells for sustainable transport, *Curr. Opin. Electrochem.*, 16, 90–95.

[6] Gittleman, C.S., Kongkanand, A., Masten, D., and Gu, W., 2019, Materials research and development focus areas for low cost automotive proton-exchange membrane fuel cells, *Curr. Opin. Electrochem.*, 18, 81–89.

[7] Chen, C., Kang, Y., Huo, Z., Zhu, Z., Huang, W., Xin, H.L., Snyder, J.D., Li, D., Herron, J.A., Mavrikakis, M., Chi, M., More, K.L., Li, Y., Markovic, N.M., Somorjai, G.A., Yang, P., and

Stamenkovic, V.R., 2014, Highly crystalline multimetallic nanoframes with three-dimensional electrocatalytic surfaces, *Science*, 343 (6177), 1339–1343.

[8] Gocyla, M., Kuehl, S., Shviro, M., Heyen, H., Selve, S., Dunin-Borkowski, R.E., Heggen, M., and Strasser, P., 2018, Shape stability of octahedral PtNi nanocatalysts for electrochemical oxygen reduction reaction studied by in situ transmission electron microscopy, *ACS Nano*, 12 (6), 5306–5311.

[9] Chi, M., Wang, C., Lei, Y., Wang, G., Li, D., More, K.L., Lupini, A., Allard, L.F., Markovic, N.M., and Stamenkovic, V.R., 2015, Surface faceting and elemental diffusion behaviour at atomic scale for alloy nanoparticles during in situ annealing, *Nat. Commun.*, 6 (1), 8925.

[10] Choi, J., Cho, J., Roh, C.W., Kim, B.S., Choi, M.S., Jeong, H., Ham, H.C., and Lee, H., 2019, Au-doped PtCo/C catalyst preventing Co leaching for proton exchange membrane fuel cells, *Appl. Catal., B*, 247, 142–149.

[11] Fidiani, E., Thirunavukkarasu, G., Li, Y., Chiu, Y.L., and Du, S., 2020, Ultrathin AgPt alloy nanorods as low-cost oxygen reduction reaction electrocatalysts in proton exchange membrane fuel cells, *J. Mater. Chem. A*, 8 (23), 11874–11883.

[12] Fidiani, E., Pravitasari, R.D., Hapsari, A.U., Budiman, A.H., Dewi, E.L., and Du, S., 2024, Porous PtAg nanowires: A highly active platinum loading electrocatalyst for oxygen reduction reaction in proton exchange membrane fuel cells, *ACS Appl. Energy Mater.*, 7, 556–564.

[13] Wang, X.X., Sokolowski, J., Liu, H., and Wu, G., 2020, Pt alloy oxygen-reduction electrocatalysts: Synthesis, structure, and property, *Chin. J. Catal.*, 41 (5), 739–755.

[14] Li, D., Wang, C., Strmcnik, D.S., Tripkovic, D.V., Sun, X., Kang, Y., Chi, M., Snyder, J.D., van der Vliet, D., Tsai, Y., Stamenkovic, V.R., Sun, S., and Markovic, N.M., 2014, Functional links between Pt single crystal morphology and nanoparticles with different size and shape: The oxygen reduction reaction case, *Energy Environ. Sci.*, 7 (12), 4061–4069.

[15] Lim, C., Fairhurst, A.R., Ransom, B.J., Haering, D., and Stamenkovic, V.R., 2023, Role of transition metals in Pt alloy catalysts for the oxygen reduction reaction, *ACS Catal.*, 13 (22), 14874–14893.

[16] Viswanathan, V., Hansen, H.A., Rossmeisl, J., and Nørskov, J.K., 2012, Universality in oxygen reduction electrocatalysis on metal surfaces, *ACS Catal.*, 2 (8), 1654–1660.

[17] Marković, N.M., Schmidt, T.J., Stamenković, V., and Ross, P.N., 2001, Oxygen reduction reaction on Pt and Pt bimetallic surfaces: A selective review, *Fuel Cells*, 1 (2), 105–116.

[18] Huang, X., Zhao, Z., Cao, L., Chen, Y., Zhu, E., Lin, Z., Li, M., Yan, A., Zettl, A., Wang, Y.M., Duan, X., Mueller, T., and Huang, Y., 2015, High-performance transition metal-doped Pt_3Ni octahedra for oxygen reduction reaction, *Science*, 348 (6240), 1230–1234.

[19] Pan, L., Ott, S., Dionigi, F., and Strasser, P., 2019, Current challenges related to the deployment of shape-controlled Pt alloy oxygen reduction reaction nanocatalysts into low Pt-loaded cathode layers of proton exchange membrane fuel cells, *Curr. Opin. Electrochem.*, 18, 61–71.

[20] Jaganmohan, M., 2024, Global nickel reserves 2023, by country, Statistics & Facts, *Statista*, https://www.statista.com/statistics/273634/nickel-reserves-worldwide-by-country/.

[21] Mardle, P., Thirunavukkarasu, G., Guan, S., Chiu, Y.L., and Du, S., 2020, Comparative study of PtNi nanowire array electrodes toward oxygen reduction reaction by half-cell measurement and PEMFC test, *ACS Appl. Mater. Interfaces*, 12 (38), 42832–42841.

[22] Mardle, P., and Du, S., 2018, Annealing behaviour of Pt and PtNi nanowires for proton exchange membrane fuel cells, *Materials*, 11 (8), 1473.

[23] Kang, Y.S., Choi, D., Park, H.Y., and Yoo, S.J., 2019, Tuning the surface structure of PtCo nanocatalysts with high activity and stability toward oxygen reduction, *J. Ind. Eng. Chem.*, 78, 448–454.

[24] Ehelebe, K., Seeberger, D., Paul, M.T.Y., Thiele, S., Mayrhofer, K.J.J., and Cherevko, S., 2019, Evaluating electrocatalysts at relevant currents in a

half-cell: The impact of Pt loading on oxygen reduction reaction, *J. Electrochem. Soc.*, 166 (16), F1259.

[25] Ehelebe, K., Schmitt, N., Sievers, G., Jensen, A.W., Hrnjić, A., Collantes Jiménez, P., Kaiser, P., Geuß, M., Ku, Y.P., Jovanovič, P., Mayrhofer, K.J.J., Etzold, B., Hodnik, N., Escudero-Escribano, M., Arenz, M., and Cherevko, S., 2022, Benchmarking fuel cell electrocatalysts using gas diffusion electrodes: Inter-lab comparison and best practices, *ACS Energy Lett.*, 7 (2), 816–826.

[26] Zhang, C., Liang, X., Xu, R., Dai, C., Wu, B., Yu, G., Chen, B., Wang, X., and Liu, N., 2021, H_2 *in situ* inducing strategy on Pt surface segregation over low Pt doped $PtNi_5$ nanoalloy with superhigh alkaline HER activity, *Adv. Funct. Mater.*, 31 (14), 2008298.

[27] Lu, Y., Du, S., and Steinberger-Wilckens, R., 2015, Temperature-controlled growth of single-crystal Pt nanowire arrays for high performance catalyst electrodes in polymer electrolyte fuel cells, *Appl. Catal., B*, 164, 389–395.

[28] Fidiani, E., AlKahfi, A.Z., Absor, M.A.U., Pravitasari, R.D., Damisih, D., Listiani Dewi, E., Chiu, Y.L., and Du, S., 2022, Au-doped PtAg nanorod array electrodes for proton-exchange membrane fuel cells, *ACS Appl. Energy Mater.*, 5 (12), 14979–14989.

[29] Fidiani, E., Thirunavukkarasu, G., Li, Y., Chiu, Y.L., and Du, S., 2021, Au integrated AgPt nanorods for oxygen reduction reaction in proton exchange membrane fuel cells, *J. Mater. Chem. A*, 9 (9), 5578–5587.

[30] El-Kharouf, A., Mason, T.J., Brett, D.J.L., and Pollet, B.G., 2012, *Ex-situ* characterisation of gas diffusion layers for proton exchange membrane fuel cells, *J. Power Sources*, 218, 393–404.

[31] Yang, Y., Zhou, X., Li, B., and Zhang, C., 2021, Recent progress of the gas diffusion layer in proton exchange membrane fuel cells: Material and structure designs of microporous layer, *Int. J. Hydrogen Energy*, 46 (5), 4259–4282.

[32] Li, M., Zhao, Z., Cheng, T., Fortunelli, A., Chen, C.Y., Yu, R., Zhang, Q., Gu, L., Merinov, B.V., Lin, Z., Zhu, E., Yu, T., Jia, Q., Guo, J., Zhang, L., Goddard, W.A.,

Huang, Y., and Duan, X., 2016, Ultrafine jagged platinum nanowires enable ultrahigh mass activity for the oxygen reduction reaction, *Science*, 354 (6318), 1414–1419.

[33] Hoshi, Y., Yoshida, T., Nishikata, A., and Tsuru, T., 2011, Dissolution of Pt-M (M: Cu, Co, Ni, Fe) binary alloys in sulfuric acid solution, *Electrochim. Acta*, 56 (15), 5302–5309.

[34] Beermann, V., Gocyla, M., Kühl, S., Padgett, E., Schmies, H., Goerlin, M., Erini, N., Shviro, M., Heggen, M., Dunin-Borkowski, R.E., Muller, D.A., and Strasser, P., 2017, Tuning the electrocatalytic oxygen reduction reaction activity and stability of shape-controlled Pt-Ni nanoparticles by thermal annealing - elucidating the surface atomic structural and compositional changes, *J. Am. Chem. Soc.*, 139 (46), 16536–16547.

[35] Zeng, W.J., Tong, L., Liu, J., and Liang, H.W., 2022, Annealing-temperature-dependent relation between alloying degree, particle size, and fuel cell performance of PtCo catalysts, *J. Electroanal. Chem.*, 922, 116728.

[36] Alia, S.M., Ngo, C., Shulda, S., Ha, M.A., Dameron, A.A., Weker, J.N., Neyerlin, K.C., Kocha, S.S., Pylypenko, S., and Pivovar, B.S., 2017, Exceptional oxygen reduction reaction activity and durability of platinum-nickel nanowires through synthesis and post-treatment optimization, *ACS Omega*, 2 (4), 1408–1418.

[37] Garsany, Y., Baturina, O.A., Swider-Lyons, K.E., and Kocha, S.S., 2010, Experimental methods for quantifying the activity of platinum electrocatalysts for the oxygen reduction reaction, *Anal. Chem.*, 82 (15), 6321–6328.

[38] Schmitt, N., Schmidt, M., Hübner, G., and Etzold, B.J.M., 2022, Oxygen reduction reaction measurements on platinum electrocatalysts in gas diffusion electrode half-cells: Influence of electrode preparation, measurement protocols and common pitfalls, *J. Power Sources*, 539, 231530.

[39] He, S., Liu, Y., Zhan, H., and Guan, L., 2021, Direct thermal annealing synthesis of ordered Pt alloy nanoparticles coated with a thin N-doped carbon

shell for the oxygen reduction reaction, *ACS Catal.*, 11 (15), 9355–9365.

[40] Simamora, R.M.A., Setyadi, J.P., Pravitasari, R.D., Arjasa, O.P., Damisih, D., Hapsari, A.U., Raharjo, J., Indayaningsih, N., Subhan, A., Budiman, A.H., Arie, A.A., and Fidiani, E., 2025, Pt nanowire arrays on graphene-integrated cathode gas diffusion layer for proton exchange membrane fuel cells, *ACS Appl. Energy Mater.*, 8 (1), 286–297.

[41] Shinagawa, T., Garcia-Esparza, A.T., and Takanabe, K., 2015, Insight on Tafel slopes from a microkinetic analysis of aqueous electrocatalysis for energy conversion, *Sci. Rep.*, 5 (1), 13801.

[42] Jia, Q., Segre, C.U., Ramaker, D., Caldwell, K., Trahan, M., and Mukerjee, S., 2013, Structure-property-activity correlations of Pt-bimetallic nanoparticles: A theoretical study, *Electrochim. Acta*, 88, 604–613.